Cogn Neurodyn (2015) 9:265–277
DOI 10.1007/s11571-015-9329-1

REVIEW PAPER

A neural network model of reliably optimized spike transmission

Toshikazu Samura · Yuji Ikegaya · Yasuomi D. Sato

Received: 29 May 2014 / Revised: 17 December 2014 / Accepted: 7 January 2015 / Published online: 23 January 2015

Abstract We studied the detailed structure of a neuronal network model in which the spontaneous spike activity is correctly optimized to match the experimental data and discuss the reliability of the optimized spike transmission. Two stochastic properties of the spontaneous activity were calculated: the spike-count rate and synchrony size. The synchrony size, expected to be an important factor for optimization of spike transmission in the network, represents a percentage of observed coactive neurons within a time bin, whose probability approximately follows a power-law. We systematically investigated how these stochastic properties could matched to those calculated from the experimental data in terms of the log-normally distributed synaptic weights between excitatory and inhibitory neurons and synaptic background activity induced by the input current noise in the network model. To ensure reliably optimized spike transmission, the synchrony size as well as spike-count rate were simultaneously optimized. This required changeably balanced log-normal distributions of synaptic weights between excitatory and inhibitory neurons and appropriately amplified synaptic background activity. Our results suggested that the inhibitory neurons with a hub-like structure driven by intensive feedback from excitatory neurons were a key factor in the simultaneous optimization of the spike-count rate and synchrony size, regardless of different spiking types between excitatory and inhibitory neurons.

Keywords Spike transmission · Power-law-distributed synchrony · Log-normally distributed synaptic weights · Synaptic background activity

Introduction

It is important to characterize the relationship between input stimulus and electrical activity of neuronal assemblies that underlie information processing in the brain (Brown et al. 2004). Such characterization is often called neural coding. Typical examples are temporal coding (Singer 2009) and phase coding (Wagatsuma and Yamaguchi 2007; Baker and Olds 2007). The firing rate (termed the spike-count rate in this work) of single neurons is also used for encoding memory in the hippocampus (Hampson et al. 2004, 2013). In fact, the hippocampus is thought to play an important role in encoding spatial information within short-term memory (Kesner 2007). To date, neural coding has been actively discussed to investigate network robustness, i.e., the sensitivity of neural responses to noise (Li and Wu 2007) and to reveal dynamical mechanisms that allow the network to correctly response to the encoded memory information as shown in Fig. 1.

T. Samura
Department of Applied Molecular Bioscience, Graduate School of Medicine, Yamaguchi University, 1-1-1, Minamikogushi, Ube, Yamaguchi 755-8508, Japan

Y. Ikegaya
Laboratory of Chemical Pharmacology, Graduate School of Pharmaceutical Sciences, The University of Tokyo, 7-3-1, Hongo, Bunkyo-ku, Tokyo 113-0033, Japan

Y. D. Sato (✉)
Frankfurt Institute for Advanced Studies (FIAS), Goethe University Frankfurt, Ruth-Moufang-Strasse. 1, Frankfurt am Main 60438, Germany
e-mail: sato@fias.uni-frankfurt.de

Y. D. Sato
Institute of Industrial Science, The University of Tokyo, 4-6-1, Komaba, Meguro-ku, Tokyo 153-8505, Japan

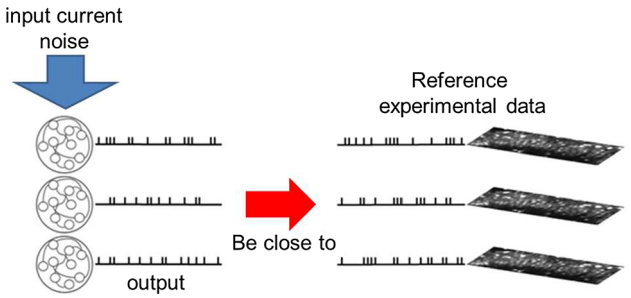

Fig. 1 The concept of optimized spike transmission in this study, referring to Shew et al. (2009, 2011). The spontaneous spike activity in the network model behaves close to the experimental reference of http://hippocampus.jp/data/ by introducing input current noise that induces synaptic background activity. The reliability of such optimized spike transmission is determined by assessing how close another network response in the model can be to the experimental reference response. (Color figure online)

A neuronal avalanche may be one of the key network behaviors necessary to understand neural coding mechanisms. In general, the neuronal avalanche is widely known as the network response that follows the power-law distribution (Beggs and Plenz 2003). The power-law distribution of the so-called synchrony size has even been observed in the hippocampus (Takahashi et al. 2010). The synchrony size, which is one of important measurements for estimating the implicit connectivity between neurons in this study, is defined as the rate of observed coactive neurons within a time bin. Previous neuronal avalanche studies have indicated that the power-law is necessary for highly efficient spike transmission in the nervous system, and that the spike transmission is optimized by appropriately balanced excitation–inhibition (Shew et al. 2011). Furthermore, dynamic range and synchrony variability are also maximized (Shew et al. 2009; Yang et al. 2012). It has been indicated that the small-world network structure referred to in Kwok et al. (2007) contributes to such optimization mechanisms (Larremore et al. 2011); however, there is less discussion about them because of the blur essence of the network structure, including the inability to accurately determine synaptic weight distribution and identify neuronal types [simply, excitatory (E) or inhibitory (I) neurons].

The power-law distribution of the synchrony size shown in Takahashi et al. (2010) was a very interesting basis for discussing the identification of neuronal types, because, as shown in Figs. 1, 2 and 3 of Takahashi et al. (2010), neurons mostly generated single spike activity. However, it is widely known that pyramidal cells (PCs) in the hippocampus intrinsically generate bursts (Jensen et al. 1996) by means of a persistent sodium current while interneurons (INs) can generate fast spikes (FSs) (Wang and Buzsáki 1996). One of the reasons why only single spike activity has been detected might be that single spikes are evoked by calcium currents, where the timescale is much slower than for sodium currents. Nevertheless, whether hippocampal PCs can generate intrinsic bursts (IBs) or single spikes has to be extensively discussed because IBs can also be evoked by calcium currents (Helmchen et al. 1999). In addition, how such spike behaviors in single neurons can affect network behaviors appears to be of significant importance for both physiological and theoretical studies (Brown et al. 2004; Miles and Wong 1983; Fujisawa et al. 2006; Steyn-Ross and Steyn-Ross 2010). For example, an early report indicated that single PCs can initiate synchronized rhythmic burst discharges in disinhibited hippocampal slices (Miles and Wong 1983). It was also demonstrated that the stimulation of single PCs could initiate a transition of the network firing state in hippocampal slices (Fujisawa et al. 2006). Macroscopic state transitions between slow wave sleep and rapid eye movement sleep were mathematically shown to be induced by stabilities of equilibria of a microscopic single neuron model undergoing saddle-node bifurcation (Steyn-Ross and Steyn-Ross 2010). Thus, it is very interesting to study the effects of neurons on network behaviors such as power-law distributions.

In recent years, it has been reported that a log-normal distribution of synaptic strength requires optimization mechanisms that maximize information capacity and transmission as mentioned above (Hiratani et al. 2013; Teramae et al. 2013). Log-normal distribution of synaptic strength is observed in neocortical slices (Song et al. 2005; Sarid et al. 2007; Lefort et al. 2009) and in the hippocampal network (Ikegaya et al. 2013). In general, the log-normal distribution with mean μ and standard deviation σ is defined as follows (Song et al. 2005):

$$p(x) = \frac{1}{\sqrt{2\pi}\sigma x}\exp\left(-\frac{(\log x - \mu)^2}{2\sigma^2}\right). \quad (1)$$

As $\sigma = 1$ and $\mu = \log(0.2) + \sigma^2$, a heavier tail indicates potentially strong-sparse and weak-dense connections in the network.

The fixed heavy-tailed distribution supports the hypothesis that the associative memory model maximizes storage capacity for memory patterns (Hiratani et al. 2013). The fixed heavy-tailed distribution of synaptic weight helps the recurrent neural network optimize spike transmission between neurons (Teramae et al. 2013). However, it is expected that such optimized spike transmission varies when the log-normal distribution also changes. In fact, the optimal spike transmission varied with changes in the strength of the same input pattern. Therefore, the detailed network structure must be understood to generate optimal spike transmission robust to the input strength, to obtain the more reliable optimal spike transmission in the network model. The heavy-tailed distribution also appears to

enhance the network response, and ensure reliable spike transmission (Ikegaya et al. 2013). However, the detailed structure of the recurrent network with a heavy-tailed distribution of synaptic weight between neurons to generate the reliable spike transmission, still remains unclear. In particular, it is unknown how the inhibitory network structure can contribute to the reliable spike transmission.

In this study, we conducted computer simulations of a network model to correctly reproduce the spontaneous activity observed in the experimental data from http://hippocampus.jp/data/. We designed a network model and performed simulations using a spiking model proposed by Izhikevich (2003, 2007). The network model consists of E and I neurons exhibiting regular spikes (RSs), or IBs and FSs. Two stochastic properties were measured from the simulations and experimental data to be analyzed. The first was the probability of the spike-count rate, and the second was the probability of the synchrony size. Using the network model subjected to synaptic background activity induced by specific input current noise, we showed that the probability of the spike-count rate for the simulations was similar to that of the experimental data. To ensure optimal and reliable spike transmission of the network model, we systematically surveyed simultaneous optimizations of the two stochastic properties in terms of different log-normal distributions of synaptic weights and specific synaptic background activity induced by the input current noise. We found that the activity of the I neurons with a hub-like structure was efficiently driven by high-frequency feedback from E neurons. In turn, E neurons were effectively suppressed by the relevant I neurons at a relatively higher frequency level. These findings suggest that log-normally distributed synaptic weights amplified the specific synaptic background activity to ensure that synchronization did not become excessive in the network model, regardless of the different spike types of E and I neurons.

A network model

Let us prepare a network model composed of $N^{\mathrm{S}}(=10)$ subnetwork models. In the sth subnetwork ($s = 1, \ldots, N^{\mathrm{S}}$), let the numbers of E and I neurons be N_s^{E} and N_s^{I}. Each neuron was defined by the original Izhikevich model (Izhikevich 2007):

$$C\frac{dv_x^{\mathrm{X}}}{dt} = k(v_x^{\mathrm{X}} - v_r)(v_x^{\mathrm{X}} - v_t) - u_x^{\mathrm{X}} + I_{\mathrm{syn}}(t) + I_{\mathrm{noise}}(t), \tag{2}$$

$$\frac{du_x^{\mathrm{X}}}{dt} = a(b(v_x^{\mathrm{X}} - v_r) - u_x^{\mathrm{X}}), \tag{3}$$

where

$$\text{if } v \geq 30, \quad \text{then} \begin{cases} v \leftarrow c \\ u \leftarrow u + d. \end{cases} \tag{4}$$

$x(=1, \ldots, N_s^{\mathrm{X}})$ is the X neuron index; $(x, \mathrm{X}) = \{(e, \mathrm{E}), (i, \mathrm{I})\}$; v_x^{X} (mV) and u_x represent the membrane potential and dimensionless variable for the membrane recovery, respectively. C is the membrane capacitance, v_r is the resting membrane potential, and v_t is the instantaneous threshold potential. k and b can be found when one knows the neuron's rheobase and input resistance, respectively (Izhikevich 2007). a is the recovery time constant. Equation (4) indicates that each neuron fires a spike when v reaches 30 mV. Then, v and u are abruptly reset to c and $u + d$, respectively. c is the voltage reset value while d is the total amount of current. In this study, when $C = 1$, $k = 0.04$, $v_r = -65$ (mV) and $v_t = -60$ (mV), Eqs. (2) and (3) are straightforwardly transformed as follows:

$$\frac{dv_x^{\mathrm{X}}}{dt} = 0.04(v_x^{\mathrm{X}})^2 + 5v_x^{\mathrm{X}} + 140 - u_x^{\mathrm{X}} + I_{rmsyn}(t) + I_{\mathrm{noise}}(t), \tag{5}$$

$$\frac{du_x^{\mathrm{X}}}{dt} = a(bv_x^{\mathrm{X}} - u_x^{\mathrm{X}}). \tag{6}$$

Equations (5) and (6) were used to reproduce different behaviors of neuron spike trains that were dependent on different values of the parameters a, b, c and d (Izhikevich 2003). To discuss whether or not network behaviors of the spike-count rate and synchrony size depend on different spike types of the single neuron, we prepared two types of network models: Identical and non-identical types. For the identical type mainly used in this study, E and I neurons were parameterized with the set of parameters representing an RS: $a = 0.02$, $b = 0.2$, $c = -65$, and $d = 8$. Meanwhile, for the non-identical type discussed in Section "Discussion and conclusion", E and I neurons were parameterized with the parameter set representing IB and FS neurons: $\{a, b, c, d\} = \{0.02, 0.2, -55, 4\}$ and $\{0.1, 0.2, -65, 2\}$, respectively.

The synaptic current $I_{\mathrm{syn}}(t)$ is described as follows:

$$I_{\mathrm{syn}} = -g_x^{\mathrm{XX}'}(v_x^{\mathrm{X}} - V_r^{\mathrm{X}}) - g_x^{\mathrm{XY}}(v_x^{\mathrm{X}} - V_r^{\mathrm{Y}}),$$

where reversal potentials $V_r^{\mathrm{E}} = 0$ (mV) and $V_r^{\mathrm{I}} = -75$ (mV), respectively. The synaptic conductances $g_x^{\mathrm{XX}'}$ and g_x^{XY} obey

$$\frac{dg_x^{\mathrm{XX}'}}{dt} = -\frac{g_x^{\mathrm{XX}'}}{\tau} + \sum_{x'} w_{xx'}^{\mathrm{XX}'} \sum_k \delta(t - t_{x'}^k - \tau_{xx'}), \tag{7}$$

$$\frac{dg_x^{\mathrm{XY}}}{dt} = -\frac{g_x^{\mathrm{XY}}}{\tau} + \sum_{y} w_{xy}^{\mathrm{XY}} \sum_k \delta(t - t_y^k - \tau_{xy}), \tag{8}$$

where (x', X') and (y, Y) are indexes representing the same and opposite synaptic types to X, e.g., when X = E, then X′ = E and Y = I. τ = 8 ms is an input time constant. $w_{xx'}^{\mathrm{XX}'}$ and w_{xy}^{XY} indicate the synaptic weights between E and I neurons, which can follow log-normal distributions. In this study, the value of the synaptic strength for E–E was randomly determined by a log-normal distribution with $\mu = \log(0.11) + \sigma^2$ for the identical type and $\mu = \log(0.17) + \sigma^2$ for the non-identical type. The synaptic strength values for E–I and I–E obeyed the log-normal distributions of $\mu = \log(W_{\mathrm{E-I}}) + \sigma^2$ and $\log(W_{\mathrm{I-E}}) + \sigma^2$. $W_{\mathrm{E-I}}$ and $W_{\mathrm{I-E}}$ varied from 0.1 to 0.4 with a step of 0.01. $\delta(\cdot)$ is the kth firing timing of the x'th presynaptic neuron. $\tau_{xx'}$, which is 1, is the synaptic delay between the xth and x'th neurons.

The input current noise term $I_{\mathrm{noise}}(t)$ takes the following form:

$$I_{\mathrm{noise}}(t) = -g_x^{\mathrm{noise}}(v_x^{\mathrm{X}} - V_r^{\mathrm{noise}}), \tag{9}$$

$$\frac{dg_x^{\mathrm{noise}}}{dt} = -\frac{g^{\mathrm{noise}}}{\tau} + w_{\mathrm{noise}}\delta(t - t_{\mathrm{noise}}^k), \tag{10}$$

where $V_r^{\mathrm{noise}} = 0(\mathrm{mV})$ and w_{noise}, which is 1, is the strength of a noise input. Intervals between noise pulses (t_{noise}^k) obey an exponential distribution with λ s. In this study, we defined two different types of input current noises that induce the relevant synaptic background activity in the network model because it has been reported that PCs fire without any synaptic events during physiological experiments (Cohen and Miles 2000). Noise A was the interval of noise input timing (t_{noise}^k) obeying the same exponential distribution (λ = 27 s) in the network model. The timing of the noise input for each neuron was randomly determined within a range of 0–5 s. This was based on experimental results, in which all connections were pharmacologically blocked in the slice cultures, wherein the distribution of the interspike intervals in the spontaneous activity obeys an exponential distribution (λ = 27 s) (Sasaki et al. 2007).

Noise B was defined as follows: the spike-count rate for each neuron was randomly determined by an exponential distribution with $\lambda = 0.25$. The spike-count rate for the xth neuron was set to be a base frequency parameter f_x. If f_x was more than 0.15, f_x was redefined by the same exponential distribution, to avoid excessive firing. Thus, the intervals between the noise input timing (t_{noise}^k) for the xth neuron obeyed an exponential distribution with $\lambda_x = 1/f_x$ s. We note that noise B is defined on the basis of a previous report that the synchronization and firing rate can be independently modulated and that external inputs affect the firing rate (Heinzle et al. 2007).

We prepared physiologically plausible network structure in the model, based on the previous experimental results. The ratio of PCs to INs was assumed to be 10:1 in the hippocampus (Traub and Miles 1991), so the number of I neurons (N_s^{I}) was set to be 10% of the E neurons, which were arranged as points on a ring lattice as shown in Fig. 2a. The I neurons were arranged with a constant distance between them on the ring. In fact, the experimental data showed that the neurons were located within the region of 250 μm by 400 μm. Neurons in the hippocampus possess axons that are longer than 1000 μm (Li et al. 1994; Gulyás et al. 1993). On the basis of these neurophysiological

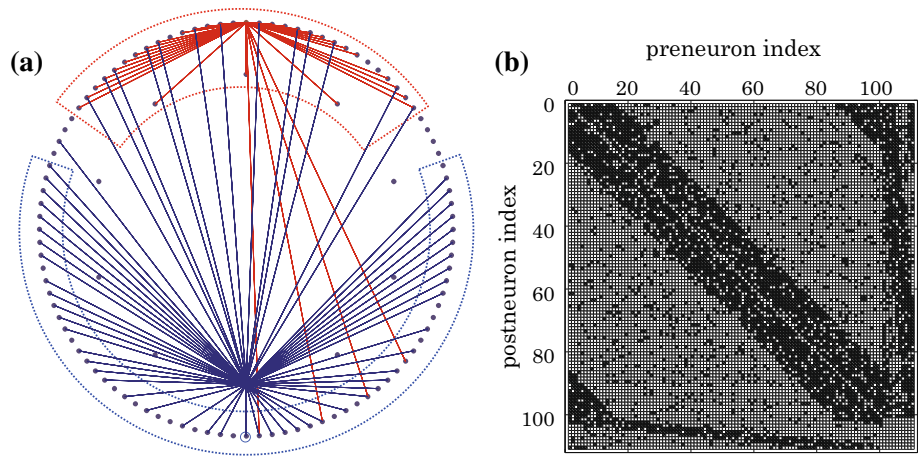

Fig. 2 Network structure of the model. **a** Arrangement and connections of each neuron. Both types of neurons are arranged on the same ring, for convenience. We plotted 100 E neurons and 10 I neurons as *black dots* on the outside and inside of the *circle*, respectively. The wired I neurons are arranged at the same position as the circled E neuron. The connections are partially drawn by *solid lines*. Each E neuron connects with the other nearest E and I neurons (*red lines*) within a certain region surrounding the postsynaptic neuron (*red box*). Each I neuron connects only with the other nearest E neurons (*blue lines*) within a certain region surrounding the postsynaptic neuron (*blue box*). However, a proportion of their connections are rewired and attached to distant neurons outside of the region. **b** Connectivity among all neurons. The *black dots* indicate the existence of connections between pre- and postsynaptic neurons. Indexes over 100th indicate I neurons in this case. (Color figure online)

experimental results, an additional assumption was included that neurons locally connect with each other and a proportion of these connections are long range (Fig. 2b). The connectivity density among PCs in a cultured slice has been shown to be 28.8 % (Takahashi et al. 2010). One E neuron thus connects to its nearest neighbor with a probability of 30 % (E–E). All I neurons were within the connection range of the E neurons (E–I). The probability of connections from the I to E neurons was 60 % (Traub and Miles 1991). The I neurons connected to the nearest E neurons (I–E) that belonged to 60 % of all of the E neurons. The connections were assumed to be rewired with a probability of 25 %. The I neurons were assumed to project only to E neurons. In addition, it was assumed that there were no inhibitory connections among the I neurons (Fig. 2b). The number of each type of connection (E–E, E–I, and I–E) was preserved before and after rewiring.

Ten subnetwork models were prepared to obtain the activity of all neurons in the model. Let N_s^{E} for each subnetwork model randomly take an arbitrary number in the range of [50, 140]. Next, we performed a simulation on the spike activity in each subnetwork model from 0 to 150 s. The spike activity was employed for 130 s out of 150 s, excluding the initial time ($<$20 s), for the sake of biological plausibility and the reliability of the simulation results. This was also done because it is difficult to claim that each subnetwork model is already in the steady state during the initial time.

The stochastic properties of the spike-count rate and synchrony size were calculated to understand how to optimize the simulation results to experimental data from http://hippocampus.jp/data/. Using the experimental data from the 14 slices, we calculated two stochastic properties of the overall spontaneous activities of the 1,193 neurons including the 141 silent neurons that could not fire during recording.

The probability of the spike-count rate represents that the number of neurons exhibiting the relevant spike-count rate is divided by the total number of neurons. The spike-count rate is also the number of spikes divided by the recording time for each neuron. The probability of any given spike-count rate smoothly decreased as frequency increased (Fig. 3a). The probability of the measured synchrony size represents the percentage of neurons exhibiting spikes in each 10-ms time bin of the entire recording duration. This was usually $<$50 %. The time bins in which no firing neurons were observed were excluded. As discussed in previous reports (Beggs and Plenz 2003; Takahashi et al. 2010; Shew et al. 2009; Yang et al. 2012; Klaus et al. 2011), this type of probability approximately obeys a power-law distribution and exhibits linearity on a log–log scale as shown in Fig. 3b.

To understand two simultaneous optimizations of the simulation results to the experimental data, the distances between the probabilities of the simulations and experimental data were calculated with a two-sample Kolmogorov–Smirnov test as referred to in Shew et al. (2009, 2011); Klaus et al. (2011). Smaller distances indicate higher similarities for the spike-count rate (or the synchrony size) between the probabilities of the experimental data and simulations.

Simulation results

To clarify the detailed network structure of the model that could optimize the stochastic property of synchrony size with high similarity for the spike-count rate calculated from the experimental data, we numerically calculated in the following procedure. First, identical subnetwork models subject to noise A were employed to reproduce the two stochastic properties of the spike-count and synchrony size for the experimental data, although there occurred a trade-off between the two stochastic properties; the optimized spike transmission in the network model was less reliable because the spike-count rate for the simulations was not similar to that for the experimental data. Second, we showed that this trade-off was eliminated when we used noise B instead of noise A in identical subnetwork models that achieved more reliably optimized spike transmission. These calculations employed the fourth-order Runge-Kutta method with a time step $\Delta t = 0.5$ ms.

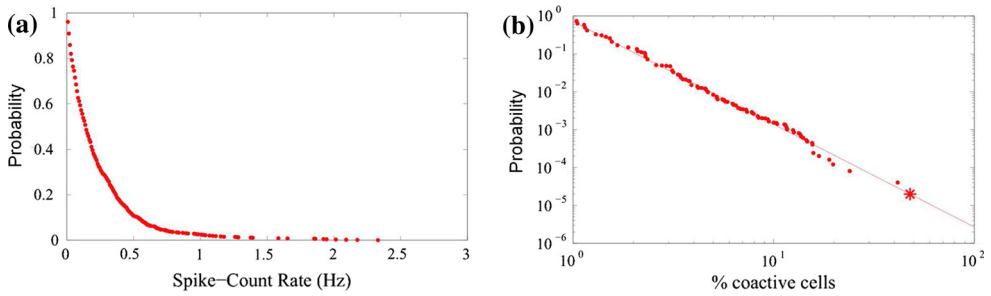

Fig. 3 Two stochastic properties of 1,193 neurons in 14 slices. **a** The probability of the spike-count rate indicates the probability of the existence of neurons that fired at a higher frequency than each spike-count rate. **b** The probability of the synchrony size. The *solid line* is the linear fit of the distribution. The *asterisk* indicates the maximum synchrony size

Trade-off in statistical properties of identical networks

Let us calculate an identical type of the network model subject to noise A. Figure 4a shows the probability of the spike-count rate for all neurons of the ten subnetwork models when all connections were removed. When the synaptic strengths of all connections were 0, noise A was applied to both the E and I neurons. The neurons fired at a low frequency (<0.1 Hz). The spike-count rate for each neuron slightly differed among the neurons. The spike-count rate for the I neurons was similar to that for the E neurons (Fig. 4b). Indeed, the I neurons were indistinguishable from the E neurons in terms of the spike-count rate that was evoked by the current noise because both types were based on the RS type of the Izhikevich model that was subject to the same current noises.

Figure 5 shows the distances between the stochastic properties of the experimental data and simulations for the rewired network model of the identical type, in which the synaptic weights obeyed log-normal distributions. The I neurons were driven by both noise A and synaptic currents from E neurons. The activity in each I neuron was delivered to the E neurons through the I–E connection. The changes in synaptic strengths (W_{E-I} and W_{I-E}) imply changes in the distances between the stochastic properties of the simulations and experimental data.

As shown in Fig. 5, the stochastic properties of the spike-count rate and synchrony size in the network model of the identical type were closer to those calculated from the experimental data with appropriate combinations of W_{E-I} and W_{I-E} to obtain the smallest distance for the probability of the spike-count rate (Fig. 5a). For the probability of the synchrony size, the distance was not yet minimized, leading to excessive synchronization compared with the experimental results (Fig. 6a). In Fig. 6b, we obtained a linear fit to the experimental results for the probability of the synchrony size. However, the probability of the spike-count rate was not simultaneously reproduced. The spike-count rate was relatively lower than the experimental results. Thus, there was a trade-off when noise A was introduced into the network model. This indicated that doubt remains about the reliability of the optimized spike transmission in the network subject to noise A.

Solving the trade-off in stochastic properties

Next, input current noise B was used to increase the spike-count rate in the right panel of Fig. 6b when the probability

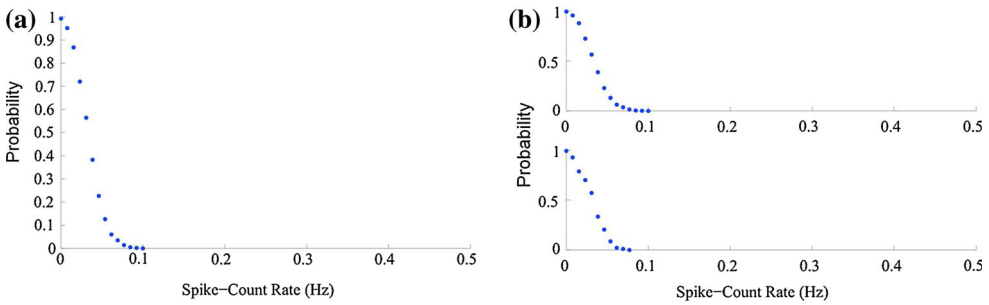

Fig. 4 Probabilities of the spike-count rate calculated in the network model of the identical type with local connectivity subjected to noise A (described above). **a** The probability of the spike-count rate calculated over all of the activities of 998 neurons in 10 trials. **b** The probability of the spike-count rate was calculated for each neuron type group (*upper panel*: E neurons, *lower panel*: I neurons)

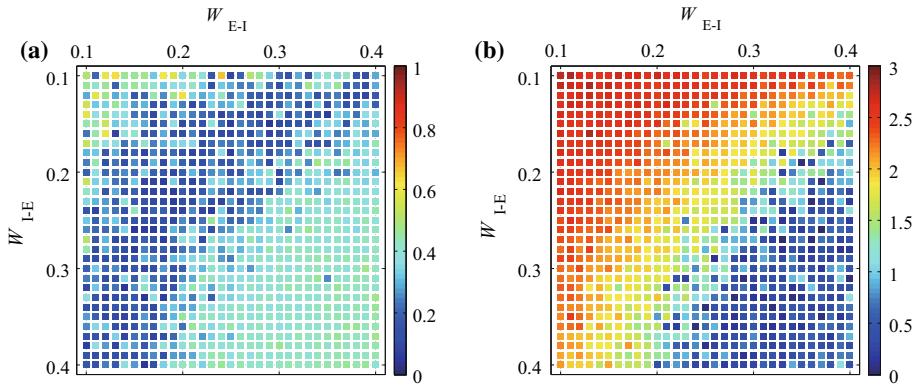

Fig. 5 Distances between the probabilities of the experimental data and the wired network model subject to noise A, in terms of parameters W_{E-I} and W_{I-E}. Each parameter was changed from 0.1 to 0.4 with 0.01 steps. **a** The probabilities of the spike-count rate. **b** The probabilities of the synchrony size

of the synchrony size for the simulations was optimized to that for the experimental data. We then examined whether or not each neuron fired with a specific spike-count rate, similar to the firing of background activity induced by noise A. Figure 7a shows the full spike-count rate for all neurons in the 10 trials of the subnetwork model without any synaptic connections. The minimum spike-count rate was almost the same, while the maximum spike-count rate increased to 0.2 Hz, compared with Fig. 4. Most of the neurons thus tended to fire at a relatively higher frequency, compared with those observed in response to noise A. Therefore, noise B seemed to cause higher background activity than noise A. The sub spike-count rates for the E and I neurons were close to each other (Fig. 7b).

For the distances between the different stochastic properties of the experimental data and rewired network model subject to noise B, we found that, for the very broad range of $(W_{\mathrm{E-I}}, W_{\mathrm{I-E}})$, the distance between the probabilities of the spike-count rate was small. However, the distance between the two probabilities of the synchrony size was the same as the results observed in response to noise A as shown in Fig. 5b. Because the probability of the spike-

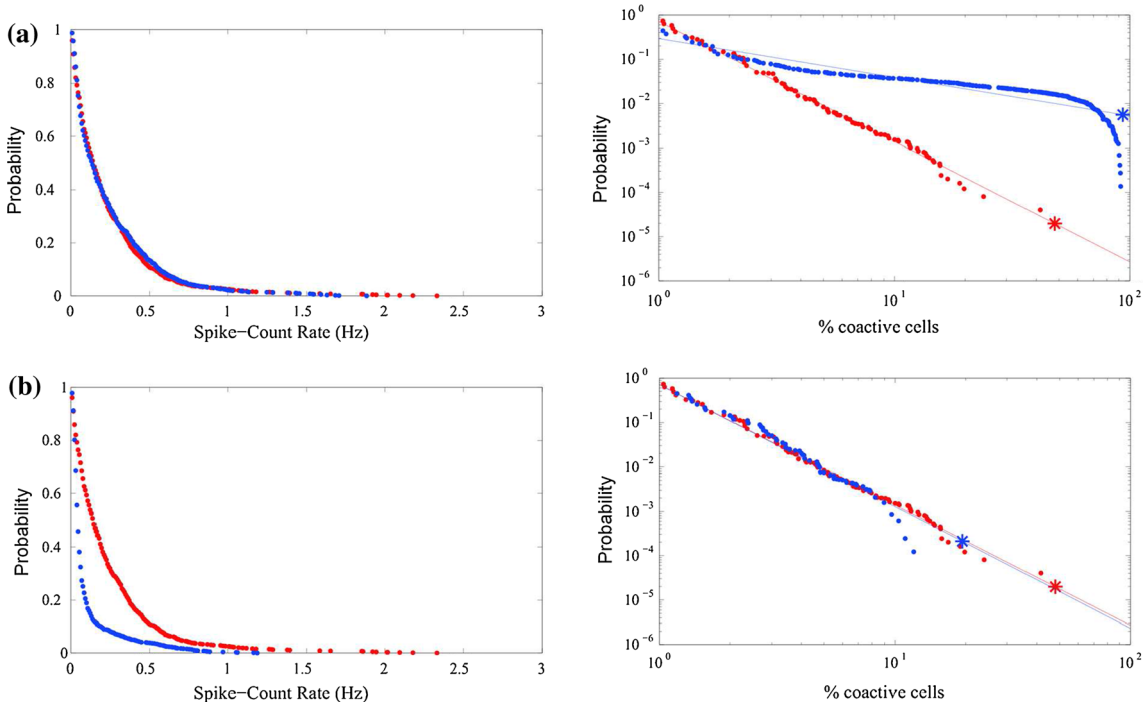

Fig. 6 The probabilities of the spike-count rate (*left*) and synchrony size (*right*). The *red* and *blue dots* indicate the probabilities of the experimental data and simulations on the rewired network model subject to noise A, respectively. The *red* and *blue lines* in the right panels indicate the linear fits of the respective results. **a** The minimal distance in the probability of the spike-count rate for $W_{\mathrm{E-I}} = 0.14$ and $W_{\mathrm{I-E}} = 0.32$, respectively. **b** The minimal distance in the probability of the synchrony size for $W_{\mathrm{E-I}} = 0.33$ and $W_{\mathrm{I-E}} = 0.27$, respectively. (Color figure online)

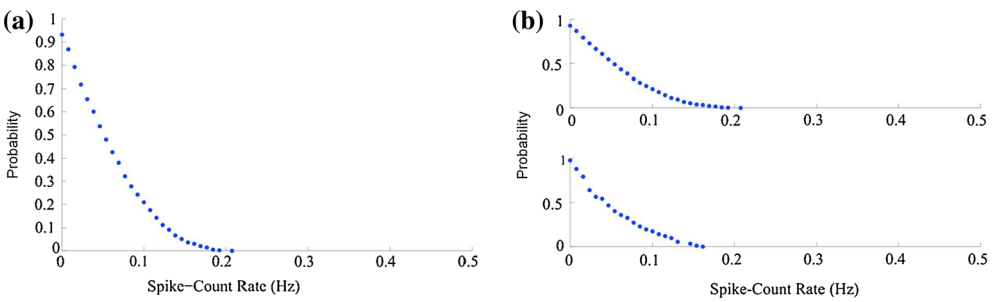

Fig. 7 Activity of all neurons obtained from the nonwired network model with noise B. **a** The probability of the spike-count rate was calculated from the activity of 1,092 neurons in 10 trials. **b** The probability of the spike-count rate of each neuron type (*upper panel*: E neurons, *lower panel*: I neurons). The neurons were classified into E and I neurons and the probabilities were calculated in each group

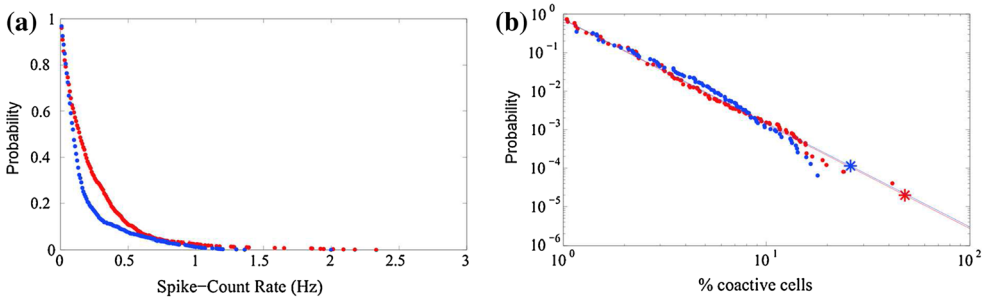

Fig. 8 The minimal distances between the probabilities of the spike-count rate (*left*) and synchrony size (*right*) when parameters $W_{E-I} = 0.26$ and $W_{I-E} = 0.36$. *Red* and *blue dots* represent the probabilities that were obtained from the experiment and simulation results, respectively. The *red* and *blue lines* indicate the linear fits of the respective results. (Color figure online)

count rate for the simulations was optimized to the probability of the spike-count rate for the experimental data, excessive synchronization was observed, similar to Fig. 6a. However, the optimal probabilities of the spike-count rate and synchrony size were found by variably balanced excitation–inhibition with $W_{E-I} = 0.26$ and $W_{I-E} = 0.36$ (Fig. 8), reducing the trade-off between the two optimizations of spike-count rate and synchrony size. We have thus addressed optimized spike transmission with high similarity for the spike count-rate.

Mechanisms to generate reliably optimal power-laws

The spike-count rate of the E neurons for the rewired network model was higher than that for the nonwired network model, regardless of the different current noise types (Fig. 4, right for noise A; Fig. 7, right and Fig. 9 for noise B). Therefore, the synaptic background activity induced by the input current noise was amplified through the E–E connection in the network model. This also optimized the spike-count rate and synchrony size that was recorded from the experimental data. Although the synaptic background activity was amplified through the E–E connection, the low-background activity induced by noise A did not optimize to the probability of the spike-count rate for the experimental data in Fig. 6b.

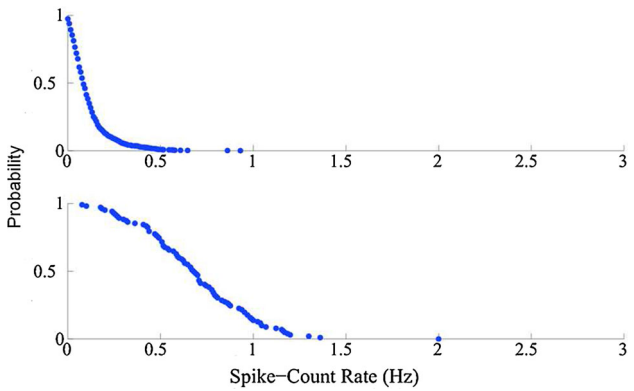

Fig. 9 The probabilities of the spike-count rate for each neuron type (*upper panel*: E neurons, *lower panel*: I neurons) in the network model subject to noise B when the distances between the two probabilities of the synchrony size were minimized with $W_{E-I} = 0.27$ and $W_{I-E} = 0.40$

Figure 10 shows the firings of a neuron during excessive or nonexcessive synchronization in the rewired network model subject to noise B. In Fig. 10a, the activity of the E neurons at arbitrary positions on the ring lattice rapidly propagated to and then activated its neighbors, among which the I neurons also fired at a high frequency. This happened when excessive synchronization emerged similar to the right panel of Fig. 6a. However, the activity of the E neurons slowly, but widely, propagated from the 90th E neuron to its neighbors in 100 ms (Fig. 10b). The number of spikes in Fig. 10b was much smaller than that in Fig. 10a. In such a condition, the probability of the synchrony size for the simulations was optimized to that for the experimental data, as shown in the right panel of Fig. 8. The main difference between excessive and nonexcessive synchronization was the synaptic strength of W_{I-E}. Let us consider two synaptic strengths of the I–E connection type $W_{I-E} = 0.15$ and 0.36. For $W_{I-E} = 0.15$, even if the I neurons fired at a high frequency, they did not sufficiently inhibit excessive activity of the E neurons. However, as the synaptic strength of the I–E connection type increased to 0.36, then the smaller number of I neurons effectively inhibited the excessive activity of the E neurons. Therefore, a strong synaptic weight for the I–E connection was necessary to create the optimized probability of synchrony size for the simulations.

Notably, the strong synaptic weights of the I–E connection were not sufficient to create an optimized probability of the synchrony size alone. We suggest that the higher frequency firings of the I neurons were necessary to find the optimized probability of the synchrony size. When the distance between the two probabilities of the synchrony size for the simulations and experimental data was minimized, the I neuron group was apparently separated from the E neuron group. This was because the I neurons fired at a higher frequency relative to the frequency level of the E

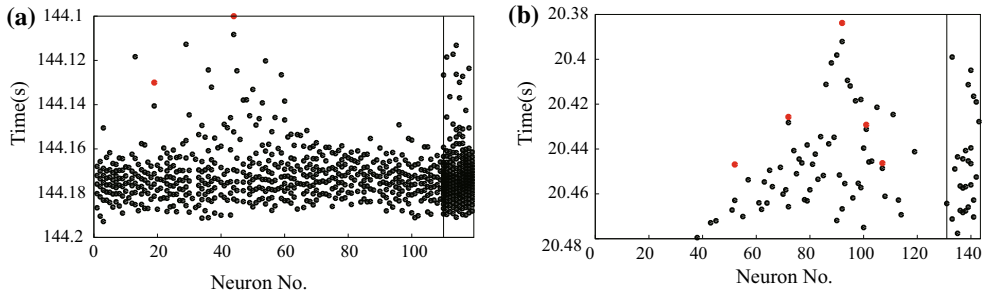

Fig. 10 Each neuron fired in excessive synchronization in the rewired network model subject to noise B. **a** Excessive synchronization occurred when $W_{E-I} = 0.33$ and $W_{I-E} = 0.15$. **b** Nonexcessive synchronization occurred when $W_{E-I} = 0.26$ and $W_{I-E} = 0.36$. The *red dots* represent the firings of neurons induced by the noise input and the *black dots* represent normal firings of neurons evoked by the synaptic inputs. The neurons on the right side are I neurons. (Color figure online)

neurons, regardless of the different noise types (see Fig. 9). Indeed, the higher frequency firings of the I neurons were driven by the E–I connection. If the synaptic strength of the E–I connection type was strong (at least, $W_{E-I} > 0.25$), then the optimized probability of the synchrony size was found. Therefore, a strong synaptic strength of the E–I connection was also necessary to efficiently drive the activity of I neurons at the higher frequency level relative to the firing frequency level of E neurons.

Finally, in order to confirm that the log-normally distributed synaptic weights of the E–I and I–E connections were of significant importance for finding the network response of the model that is similar to the stochastic properties of synchrony size and spike-count rate for experimental data, we simulated a network model in which the synaptic weights obeyed a Gaussian distribution. Let us consider W_{E-I} or $W_{I-E} > 0$ where the means and standard deviations of the Gaussian distribution were set to be the same as those of the log-normal distribution for each connection type, W_{E-I} or W_{I-E}. The distances for each stochastic property were individually minimized on the (W_{E-I}, W_{I-E}) diagram. However, the stochastic properties of the spike-count rate and synchrony size did not simultaneously achieve their best fit to those for the experimental data. This indicated that the log-normal distribution rather than the Gaussian distribution of the synaptic weight was of importance for simultaneously finding both the optimized probabilities of the synchrony size and spike-count rate, because the synaptic background activity, which is induced by the specific input current noise in the network model, was not incremented aside from that observed for the log-normally distributed synaptic weight.

Discussion and conclusion

In this study, we described how the spontaneous activity of the network model was reliably optimized to that of the experimental data. These results suggest that the balances of the log-normal distributions of the synaptic weights and synaptic background activity induced by input current noise with a base frequency below 0.15 play important roles in optimizing stochastic properties. The background activity was driven through the E–E connection in the network model. Thus, the log-normally distributed synaptic weights also enhanced the synaptic background activity such that the probability of the spike-count rate for the simulations was optimized to that for the experimental data. The amplified synaptic background activity supported the idea that the nonexcessive synchrony size for the simulations optimized the probabilities for the experimental data. This also addressed the issue that the strong synaptic weights of the E–I and I–E connection types were necessary for driving the I neurons at a higher frequency relative to the frequency level of the E neurons and for effectively propagating one E neuron to its neighbors (Fig. 10b).

Using our network model, we showed that the background activity was driven from the low to high frequency levels through the strong E–E connections. Then, the probability of the spike-count rate was optimized to that for the experimental data. These results may support the experimental fact that the activity of a single neuron can entrain the hippocampal population (Smith et al. 1995). However, in our network model without any connections, we could not show that the low-frequency background activity was able to reproduce the spontaneous activity that was observed in the pharmacologically blocked slice cultures of Sasaki et al. (2007). This may indicate that such a pharmacological block significantly harms the normal background activity of the slice cultures, and decreases its overall frequency level.

It has been suggested that the activity of some neurons causes firing of other nearby neurons and that the relevant excitatory cascade induces synchronization in the entire CA3 network when inhibitory neurons are suppressed (Smith et al. 1995). It has also been reported that most of the neurons that simultaneously fire within a time bin of 10

ms were not observed in the slice cultures (Takahashi et al. 2010). These experimental results may be supported by our network model, because it can easily drive all the neurons by amplifying the synaptic background activity through the variable log-normal distributions of the synaptic weights for the E–I and I–E connections. The appropriate log-normal distribution of the synaptic weight prevented excessive activity in the present network model. Thereby, the present network model confirmed that the activity of I neurons was efficiently driven by the E–I connection. This also implied that I neurons, which fire at a higher frequency than E neurons, were predominant in the high-frequency range of the network activity. Notably, the strong I–E connections were necessary to effectively inhibit E neurons in the present network model.

Changeably balanced E–I and I–E connectivities in our network model were supported by some of the experimental results. It has been reported that the firing of inhibitory neurons is preceded by excitatory postsynaptic potentials (EPSPs) in hippocampus (Cohen and Miles 2000). Some of the GABAergic INs, which are considered to be inhibitory, connect to many of the other neurons in hippocampus through functional synaptic connections. In this sense, activity in the hippocampal region is significantly decreased by the activity of superconnected GABAergic INs (Bonifazi et al. 2009). The superconnected GABAergic INs intensively receive many spontaneous EPSPs. Their threshold for an action potential is low (Bonifazi et al. 2009). Therefore, this indicates that the aforementioned hub-like structure of the I neurons with effective E–I connections exist in the hippocampal network. Let us model INs as the FS type, which fired more frequently in the network in the experiment (Smith et al. 1995). Since such INs tend to fire frequently, compared to the RS type, we can expect that the high activity of inhibitory neurons suppresses excessive synchronization and creates the optimized probability of the synchrony size.

To establish a more biologically plausible network model, we need to discuss more which PC spike type, a single spike or a burst, is more plausible. Our network model was established based on the experimental data of Takahashi et al. (2010), where neurons unidentified as PCs or INs exhibited single spikes. However, another experiment has demonstrated increases in intracellular calcium at the time of burst firing (Helmchen et al. 1999). Additionally, hippocampal PCs and INs have often been computationally modeled as a burst of spikes and an FS, respectively (Wang and Buzsáki 1996; Tateno et al. 1998; Yoshida et al. 2002).

Thus, we study how the spike-count rate varies with or without connections between E and I neurons in a non-identical type of the network model. When the synaptic strengths of all connections were 0 and noise A was applied to both the E and I neurons, the neurons fired at a low frequency (<0.4 Hz). We obtained the probability curve of the spike-count rate, which was similar to that for the identical type in Fig. 4a. Next, let us consider the case for $W_{\mathrm{E-I}} = 0.34$ and $W_{\mathrm{I-E}} = 0.17$. In this case, the E neurons effectively enhance the frequency of firing in the I neurons, while the I neurons properly suppress spike activity of the E neurons. We thus found that the I neurons fired at a higher frequency relative to the E neurons. In addition, for the spike-count rate, the probability curve for the simulations properly replicated that of the experimental data of Fig. 4b. Such replication is expected to be obtained as follows: First, the two stochastic properties could be simultaneously optimized to those for the experimental data if the synaptic background activity and the log-normally distributed synaptic weight changed. Second, the two optimizations were independent of the different spike behaviors of E and I neurons. Indeed, the probability of the spike-count rate is considered to be replicated by the specific property of the IB neuron in the non-identical type of the network model. Since the IB type fires an initial burst of spikes followed by repetitive single spikes, in calculating the probability of the spike-count rate, the data in the initial time (< 20 s), which possibly contain the burst of spikes, were excluded to obtain a qualitatively similar probability to that for the experimental data. Furthermore, as shown in Fig. 2 of Izhikevich (2003), the RS and IB types were prepared with the same set of parameters (a, b) and had similar nonlinearity. This is almost the same for the I neurons of the RS and FS types.

The chattering (CH) type can also be used to describe the burst of spikes in the E neurons. Even if the CH type is employed in our network model, we would expect to obtain similar results to the two simultaneous optimizations described here because there are few differences between the dynamical properties of the CH, RS, and IB types with the same set of (a, b) parameters. In addition, we assume that the first spike of the burst is only counted as a spike in calculations of the spike-count rate and synchrony size. This is expected to allow us to obtain the two stochastic properties for CH, similar to those found in this study. Even if we consider all spikes in the burst from the E neurons, rather than only the first, as synaptic inputs to the I neurons, this means that the I neurons receive synaptic inputs with higher frequency from the E neurons for the CH type, relative to those for the IB and RS types. In particular, for the CH type, the weaker synaptic weight of the E–I was thus expected to be simultaneously optimized to the two stochastic properties of the experimental data. For the I neurons, let the RS type change to the FS one. The spike-count rate for the FS type is higher than that for the RS type. This indicates that the weaker synaptic weight of the I–E helps more effective optimizations of the two

stochastic properties to the experimental data. Therefore, these discussions suggest that the two simultaneous optimizations of the stochastic properties are not dependent on the different neuronal types, rather, they significantly rely on the amplified synaptic background activity and the changeable log-normal distribution of the synaptic weight.

Let us briefly mention the reason why we did not use the original Izhikevich model in this study. The improved version of the Izhikevich model is not so complicated. In addition, it is convenient and helpful for studying different spike behaviors in a single neuron, compared with the original version. Even if the original Izhikevich model described in Eqs. (2)–(4) is used, it would be difficult for us to identify dynamical mechanisms for each spike behavior, because we have to firstly study bifurcation characteristics hidden in the spike behaviors with the complicated phase diagram of many intrinsic parameters, referring to in Touboul and Brette (2009), Shlizerman and Holmes (2012). On the other hand, the simplified versions of Eqs. (5) and (6) can more easily specify spike behaviors with phase diagrams of less intrinsic parameters in Fig. 2 of Izhikevich (2003). We have thus concluded that two optimizations for the spike-count rate and synchrony size are independent of different spike types, at least, a single spike or a burst, as mentioned above.

We can expect that the signal-to-noise ratio is reduced when the synaptic background activity is amplified. However, this should be further discussed, in terms of dynamic range, which is a network response to ranges of intrinsic and extrinsic stimulus amplitudes. The simulations in this work predict that, at criticality, a network model will optimize with the experimental data of the power-law-distributed synchrony size, after which it will exhibit excessive synchronization as the synaptic background activity is gradually amplified. This implies that the signal-to-noise ratio is also maximized at the criticality and is then reduced with further amplification of background activity. These results are similar to those in Shew et al. (2009), Larremore et al. (2011), Kinouchi and Copelli (2006). Compared to such previous results for maximized dynamic range, we can confirm that the amplified synaptic background activity in our network model plays a crucially important role in optimizing the power-law-distributed synchrony size.

Let us discuss the functional roles of the INs in reliably optimized spike transmission in the hippocampal circuit. We observed simultaneous optimizations of two stochastic properties controlled by a log-normal distribution of the synaptic weight for E–I and I–E in an identical network model with noise B. This is thought to indicate that high frequency activity of the I neurons with a hub-like structure play important roles in reliably optimized spike transmission, because, in Teramae et al. (2013), optimal spike transmission is demonstrated with different internal noise values. Nevertheless, the reliability of optimal spike transmission still remains unknown. We can predict that different log-normal distributions of the synaptic weight induce different optimized spike transmissions. There remains ample discussion about the functional roles of the I neurons in the reliably optimized spike transmission.

In Shew et al. (2009), optimized spike transmission was found by calculating Shannon entropy and the mutual information. However, it remained unclear the detailed network structure, with a log-normal distribution of synaptic weight and I neurons, hidden in the optimized spike transmission. Compared with previous works, our network model confirmed details of the functional role of the I neurons with a hub-like connection structure in reliable optimization of the synchrony size by controlling a log-normal distribution of synaptic weight and input current noise that induces synaptic background activity. Because our network model can even predict the structure that will maximize information capacity and transmission by calculating Shannon entropy and mutual information, we have provided evidence supporting our hypothesis that our network model is the most effective memory network exhibiting firing patterns similar to those stored in associative memory. In addition, our model may be useful and helpful to understand the functional roles of the I neurons in transitions to seizures, because it was previously shown that synchrony size increases together with the high-frequency activity of I neurons prior to epileptic seizure onset (Jiruska et al. 2010).

Since our network model is biologically plausible, it may be very similar to the architectures proposed by Traub and Miles (1991) and Taxidis et al. (2012, 2013). One of the main differences between our model and theirs is that a log-normal distribution of synaptic weight is introduced. Using a more biologically plausible network model, we found that the log-normally distributed synaptic weight and activity of the inhibitory neurons play important roles in optimizing the stochastic properties of synchrony size and spike-count rate. In this sense, if the log-normally distributed synaptic weight can also be applied to the CA3-CA1 network model proposed by Taxidis, it may become clear how the log-normal distribution of synaptic weight can affect oscillations in the hippocampus. In addition, because the synchrony size optimized by the log-normal distribution of synaptic weight is implicitly related to maximized spike transmission in the hippocampus, it might clarify how sharp wave-ripple complexes can contribute to memory processing in the hippocampus during deep sleep.

In conclusion, we studied the network response of a model for optimized spike transmission, to discuss the reliability of such optimized spike transmission for

information processing. In this study, we calculated two stochastic properties, the spike-count rate and the synchrony size. We systematically investigated how each stochastic property could be optimized to that calculated from the experimental data, in terms of different spike types, a log-normally distributed synaptic weight, and synaptic background activity in the network model. We found that optimizations of the spike-count rate and synchrony size did not seem to depend on the different spike types of E and I neurons. The two simultaneous optimizations significantly depended not only on the changeably balanced log-normal distribution of synaptic weight between E and I neurons, but also on appropriately amplified synaptic background activity induced by specific input current noise. Moreover, we found a hub-like network structure of I neurons, in which the I neurons were driven by intensive feedback from E neurons, and at the same time effectively suppressed the E neurons. Our results indicate that the optimized probability of the spike-count rate support highly reliable optimized spike transmission in the network model.

Acknowledgments Y. D. S. was partially supported by a Grant-in-Aid for Challenging Exploring Research No. 25540110. Y. I. was partially supported by the Funding Program for Next Generation World-Leading Researchers (No. LS023).

References

Baker JL, Olds JL (2007) Theta phase precession emerges from a hybrid computational model of a CA3 place cell. Cogn Neurodyn 1(3):237–248

Beggs JM, Plenz D (2003) Neuronal avalanches in neocortical circuits. J Neurosci 23(35):11167–11177

Bonifazi P, Goldin M, Picardo MA, Jorquera I, Cattani A, Bianconi G, Represa A, Ben-Ari Y, Cossart R (2009) GABAergic hub neurons orchestrate synchrony in developing hippocampal networks. Science 326(5958):1419–1424

Brown EN, Kass RE, Mitra PP (2004) Multiple neural spike train data analysis: state-of-the-art and future challenges. Nat Neurosci 7(5):456–461

Brown E, Moehlis J, Holmes P (2004) On the phase reduction and response dynamics of neural oscillator populations. Neural Comput 16:673–715

Cohen I, Miles R (2000) Contributions of intrinsic and synaptic activities to the generation of neuronal discharges in in vitro hippocampus. J Physiol 524(Pt 2):485–502

Fujisawa S, Matsuki N, Ikegaya Y (2006) Single neurons can induce phase transitions of cortical recurrent networks with multiple internal states. Cereb Cortex 16(5):639–654

Gulyás AI, Miles R, Hájos N, Freund TF (1993) Precision and variability in postsynaptic target selection of inhibitory cells in the hippocampal CA3 region. Eur J Neurosci 5(12):1729–1751

Hampson RE, Pons TP, Stanford TR, Deadwyler SA (2004) Categorization in the monkey hippocampus: a possible mechanism for encoding information into memory. Proc Natl Acad Sci USA 101(9):3184–3189

Hampson RE, Song D, Opris I, Santos LM, Shin DC, Gerhardt GA, Marmarelis VZ, Berger TW, Deadwyler SA (2013) Facilitation of memory encoding in primate hippocampus by a neuroprosthesis that promotes task-specific neural firing. J Neural Eng 10(6):066013

Heinzle J, König P, Salazar RF (2007) Modulation of synchrony without changes in firing rates. Cog Neurodyn 1:225–235

Helmchen F, Svoboda K, Denk W, Tank DW (1999) In vivo dendritic calcium dynamics in deep-layer cortical pyramidal neurons. Nat Neurosci 2(11):989–996

Hiratani N, Teramae JN, Fukai T (2013) Associative memory model with long-tail-distributed Hebbian synaptic connections. Front Comput Neurosci 6:102

Ikegaya Y, Sasaki T, Ishikawa D, Honma N, Tao K, Takahashi N, Minamisawa G, Ujita S, Matsuki N (2013) Interpyramid spike transmission stabilizes the sparseness of recurrent network activity. Cereb Cortex 23(2):293–304

Izhikevich EM (2003) Simple model of spiking neurons. IEEE Trans Neural Netw 14:1569–1572

Izhikevich EM (2007) Dynamical systems in neuroscience: the geometry of excitability and bursting. MIT Press, Cambridge, MA

Jensen MS, Azouz R, Yaari Y (1996) Spike after-depolarization and burst generation in adult rat hippocampal CA1 pyramidal cells. J Physiol 492:199–210

Jiruska P, Csicsvari J, Powell AD, Fox JE, Chang WC, Vreugdenhil M, Li X, Palus M, Bujan AF, Dearden RW, Jefferys JG (2010) High-frequency network activity, global increase in neuronal activity, and synchrony expansion precede epileptic seizures in vitro. J Neurosci 30(16):5690–5701

Kesner RP (2007) Behavioral functions of the CA3 subregion of the hippocampus. Learn Mem 14(11):771–781

Kinouchi O, Copelli M (2006) Optimal dynamical range of excitable networks at criticality. Nat Phys 2:348–351

Klaus A, Yu S, Plenz D (2011) Statistical analyses support power law distributions found in neuronal avalanches. PLoS one 6(5):e19779

Kwok HF, Jurica P, Raffone A, van Leeuwen C (2007) Robust emergence of small-world structure in networks of spiking neurons. Cogn Neurodyn 1(1):39–51

Larremore DB, Shew WL, Restrepo JG (2011) Predicting criticality and dynamic range in complex networks: effects of topology. Phys Rev Lett 106(5):058101

Lefort S, Tomm C, Floyd Sarria JC, Petersen CC (2009) The excitatory neuronal network of the C2 barrel column in mouse primary somatosensory cortex. Neuron 61(2):301–316

Li XG, Somogyi P, Ylinen A, Buzsáki G (1994) The hippocampal CA3 network: an in vivo intracellular labeling study. J Comp Neurol 339(2):181–208

Li S, Wu S (2007) Robustness of neural codes and its implication on natural image processing. Cogn Neurodyn 1(3):261–272

Miles R, Wong RKS (1983) Single neurones can initiate synchronized population discharge in the hippocampus. Nature 306:371–373

Sarid L, Bruno R, Sakmann B, Segev I, Feldmeyer D (2007) Modeling a layer 4-to-layer 2/3 module of a single column in rat neocortex: interweaving in vitro and in vivo experimental observations. Proc Natl Acad Sci USA 104(41):16353–16358

Sasaki T, Matsuki N, Ikegaya Y (2007) Metastability of active CA3 networks. J Neurosci 27(3):517–528

Shew WL, Yang H, Petermann T, Roy R, Plenz D (2009) Neuronal avalanches imply maximum dynamic range in cortical networks at criticality. J Neurosci 29(49):15595–15600

Shew WL, Yang H, Yu S, Roy R, Plenz D (2011) Information capacity and transmission are maximized in balanced cortical networks with neuronal avalanches. J Neurosci 31(1):55–63

Shlizerman E, Holmes P (2012) Neural dynamics, bifurcations, and firing rates in a quadratic integrate-and-fire model with a recovery variable. I: deterministic behavior. Neural Comput 24(8):2078–2118

Singer W (2009) Distributed processing and temporal codes in neuronal networks. Cogn Neurodyn 3(3):189–196

Smith KL, Szarowski DH, Turner JN, Swann JW (1995) Diverse neuronal populations mediate local circuit excitation in area CA3 of developing hippocampus. J Neurophysiol 74(2):650–672

Song S, Sjöström PJ, Reigl M, Nelson S, Chklovskii DB (2005) Highly nonrandom features of synaptic connectivity in local cortical circuits. PLoS Biol 3(3):e68

Steyn-Ross DA, Steyn-Ross M (2010) Modeling phase transitions in the brain. Springer, New York

Takahashi N, Sasaki T, Matsumoto W, Matsuki N, Ikegaya Y (2010) Circuit topology for synchronizing neurons in spontaneously active networks. Proc Natl Acad Sci USA 107:10244–10249

Tateno K, Hayashi H, Ishizuka S (1998) Complexity of spatiotemporal activity of a neural network model which depends on the degree of synchronization. Neural Netw 11(6):985–1003

Taxidis J, Coombes S, Mason R, Owen MR (2012) Modeling sharp wave-ripple complexes through a CA3-CA1 network model with chemical synapses. Hippocampus 22(5):995–1017

Taxidis J, Mizuseki K, Mason R, Owen MR (2013) Influence of slow oscillation on hippocampal activity and ripples through cortico-hippocampal synaptic interactions, analyzed by a cortical-CA3-CA1 network model. Front Comput Neurosci 7:3

Teramae JN, Tsubo Y, Fukai T (2013) Optimal spike-based communication in excitable networks with strong-sparse and weak-dense links. Sci Rep 2:485

Touboul J, Brette R (2009) Spiking dynamics of bidimensional integrate-and-fire neurons. SIAM J Appl Dyn Syst 8(4):1462–1506

Traub RD, Miles R (1991) Neuronal networks of the hippocampus. Cambridge Univ Press, Cambridge

Wagatsuma H, Yamaguchi Y (2007) Neural dynamics of the cognitive map in the hippocampus. Cogn Neurodyn 1(2):119–141

Wang XJ, Buzsáki G (1996) Gamma oscillation by synaptic inhibition in a hippocampal interneuronal network model. J Neurosci 16(20):6402–6413

Yang H, Shew WL, Roy R, Plenz D (2012) Maximal variability of phase synchrony in cortical networks with neuronal avalanches. J Neurosci 32(3):1061–1072

Yoshida M, Hayashi H, Tateno K, Ishizuka S (2002) Stochastic resonance in the hippocampal CA3-CA1 model: a possible memory recall mechanism. Neural Netw 15(10):1171–1183